Stalling and Dissipation of a Near-Inertial Wave (NIW) in an Anticyclonic Eddy: Direct Determination of Group Velocity and Comparison with Theory

Thomas B. Sanford[1,2], Barry B. Ma[1], and Matthew H. Alford[3]

[1]Appled Physics Laboratory, University of Washington

[2]School of Oceanography, University of Washington

[3]Scripps Institution of Oceanography, University of California San Diego

Corresponding author: Thomas B. Sanford (sanford@apl.uw.edu)

Key Points

- Profilers observe mesoscale vorticity and vertical shear and support computations of NIW's phase and group velocities from 1st principles
- First known determination of NIW vertical group velocity computed from $\partial\omega/\partial m$ in ocean observations
- Analytic theory that incorporates both mesoscale vorticity and vertical shear predicts NIW kinetic properties that compares well with observations
-

Index terms: Coriolis effects, Internal and inertial waves, Turbulence, Diffusion and mixing processes

Key words: NIW, near-inertial, mesoscale eddy, intrinsic frequency, critical layer, group velocity

Abstract

Nearly-Lagrangian observations from two EM-APEX velocity and density profiling floats on concentric trajectories determine profiles of ocean eddy vorticity and velocity, and the intrinsic frequency, energy, vertical wavenumber, vertical phase velocity, and vertical group velocity of a near-inertial-wave (NIW). For the first time, NIW C_{pz} and C_{gz} are computed from first principles (by direct computation of ω_i/m and $\partial\omega_i/\partial m$ vs. depth without a dispersion relation). This novel experiment, moving with turbulent zone produced by a downgoing NIW packet observed stalling at 135-m depth. KE flux convergence initiates KE dissipation at 115 m. Below 135 m, shear production is hypothesized to support dissipation. These observations compare well with a theory of NIW interaction with the eddy, not in solid-body rotation. Theory and

observations show that the observed turbulent zone arises from wave stalling and instability in a critical or caustic layer as the vertical group velocity of the wave goes toward zero.

Plain Language Summary

A subsurface zone of turbulence was observed for a week by a pair of autonomous velocity and density profilers on concentric paths in an ocean eddy. In this novel experiment, our profilers moved with the turbulent zone, providing a new view of the turbulence's 3D and temporal structure. The profilers also provided estimates of the eddy's vertical vorticity and shear, quantities needed to test a new formulation of downward NIW energy flux and loss from inertial wave–eddy interactions. The unique observations of the wave's intrinsic frequency ω_i and vertical wavenumber m provide an estimate of the vertical group velocity from changes in ω_i with respect to m. Convergence of the energy flux, initiated turbulence and KE dissipation. To our knowledge, such observations and evaluations have not been made before. Observed quantities compare well with a theory of inertial wave–eddy interactions. This study may improve our understanding of how deep-water mixing occurs and how better to model the effects globally.

1. Introduction

Near-inertial waves (NIW) contain a significant fraction of the ocean's internal wave energy and shear (Weller, 1982; Alford et al., 2017). The unique aspects of NIWs are discussed by Garrett (2001). While they are known to contribute to ocean turbulence (Hebert & Moum, 1994; Alford & Gregg, 2001, Whalen et al., 2018), the importance of NIW turbulence production relative to other mechanisms is unknown (Alford et al., 2016). Extensive research has focused on NIW generation and propagation, much of it reviewed or cited by Alford et al. (2016) and Kawaguchi et al. (2016, 2020).

An important potential means of NIW dissipation is the trapping or stalling of NIWs in mesoscale ocean eddies and fronts. Contrary to the classic low-frequency limit for propagating internal waves f (the Coriolis frequency), theory and observations show that the lower frequency limit for freely propagating internal waves is modified by the mean background vertical vorticity and vertical shear. An anticyclonic part of a front or mesoscale eddy will reduce the effective $f(z)$, producing a depth-variable lower limit to NIW propagation. Ocean mesoscale eddies are usually strongest on the surface, creating the possibility for downgoing waves to stall when they reach the lower edge of the waveguide. Mooers (1975) derives the limiting frequency of a NIW in a mesoscale front as $f(f + \zeta)^{1/2}$. Kunze (1985) demonstrated with ray tracing the trapping and amplification of NIW in geostrophic jet. Kunze et al. (1995) and Whitt & Thomas (2013) identify the added effect of mean baroclinicity, i.e., mean flow with vertical shear. Joyce et al. (2013) formulate an expression for the limiting frequency of inertial-gravity waves in a mesoscale ocean vortex in gradient wind balance.

Our brief report focuses on the progress of NIWs studies from autonomous, quasi-Lagrangian, free-fall velocity profilers. This observational technique was first reported by Rossby (1969) and Drever and Sanford (1970). Rossby and Sanford (1976) used their newly developed velocity profilers in 1971 to describe for the first time high-resolution vertical profiles of the velocity, group velocity, and energy flux of NIW motions. The highly resolved, repeated profiles reveal structure not captured by widely separated moored current meters. Significant additional total water column profiles of NIWs were obtained by free-falling, motional-induction profilers in the 1972 MODE and 1978 POLYMODE experiments (Sanford, 1975; Leaman & Sanford, 1975; Sanford, 2013). Expendable current profilers (XCPs) have been deployed from underway vessels into ocean fronts and eddies (D'Asaro & Perkins, 1984; Kunze & Sanford, 1984; D'Asaro, 1985; Kunze & Lueck, 1986; Kunze et al., 1995; Kunze & Toole, 1997). Other methods exhibited high resolution velocity profiles in NIWs, such as Pegasus (Spain et al.,1981), ship lowered ADCPs (Visbeck, 2002), drifting *FLIP* (Pinkel, 1984), drifting cable crawlers, such as WireWalker (Pinkel et al., 2011) and MMP (e.g., Alford, 2010.

The observations and analyses presented here have several unique and/or novel aspects:

(1) Quasi-Lagrangian timeseries measurements, as the profiling floats moved with the turbulent zone, support computation of profiles of NIW intrinsic frequency ω_i and vertical wavenumber m, and mesoscale eddy vertical shear and vorticity.

(2) NIW ω_i and m are computed from time rate of change of NIW direction and its vertical gradient, respectively.

(3) For the first time, vertical group velocity is computed directly as $\partial \omega_i / \partial m$ (Lighthill, 1978), without recourse to a dispersion relation.

(4) Vertical group velocity and energy density provide an estimate of NIW vertical energy flux and its vertical gradient.

(5) Observations from two continuously profiling EM-APEX floats on nearly concentric paths provide areal-averaged vorticity profiles computed by the Kelvin circulation theorem ζ_0 and solid body rotation $2V_0 / r_0$, respectively.

(6) Observations are compared favorably to comprehensive mesoscale eddy–NIW interaction theory for a non-solid body rotating eddy (Joyce et al., 2013).

2. Methods and Observations

2.1. Methods

The EM-APEX, an autonomous ocean velocity and density profiling float (Sanford et al., 2005) manufactured by Teledyne Webb Research Corp., observes a velocity profile inferred from voltages induced by the motion of the float and the surrounding seawater through the Earth's magnetic field (Sanford et al., 1978). The observed motionally-induced voltage is interpreted as $v(z,t) - \overline{v}^*(t)$. Although time dependent, $\overline{v}^*$ is generally only slowly variable, because it is a water-column-averaged quantity (Sanford, 1971). The absolute ocean velocity profile is obtained with the compensation for $\overline{v}^*$ through the difference between the GPS positions between the start and end of a profile and the time integrated EM-APEX relative velocity during the submerged profile. The absolute velocity is used for all analyses in this paper. The profile profiles up and down at 0.1-0.15 m s^{-1}, yielding profiles that passed through 150 on down and up traverses with time differences of between 40 and 55 min apart.

The onboard processing is standard for velocity, based on a 50-s fit to the 1-s electric field values. The fit is moved 25 s and repeated, yielding a depth interval of 2–3 m. The profiles are gridded to 2-m levels and 1-h intervals. The 1-s values of electric field, converted to ocean velocity, are treated as velocity variance on scales ≤ 5 m, which is interpreted as turbulent kinetic energy and termed TKE$_5$. TKE$_5$ has been shown to measure surface gravity wave velocities amplitudes (Sanford et al, 2007; Hsu et al., 2018).

The floats measure the ocean temperature and salinity as a function of depth with a Sea-Bird Electronics 41 CTD. The vertical sample rate is 2–3 m and gridded to the same depth and time intervals as velocity values.

2.2. Observations

Two EM-APEX floats were deployed in the SW Sargasso Sea of the NW Atlantic Ocean in May–June 2016 in proximity to the Gulf Stream amid strong mesoscale eddies with hourly observations extended over the upper 300 m (Figure 1).

Notable features are the anticyclonic circulation of the floats, numerous salinity interleavings, density levels about 50-m shallower observed by float 7792, and strong NIW energy density observed by float 7793, though not by 7792. The stable distribution of properties supports the model of the NIW superimposed on subinertial properties that are predominately spatially, not temporally variable. This is a frozen field assumption for the background flow, which will be assumed in subsequent analyses.
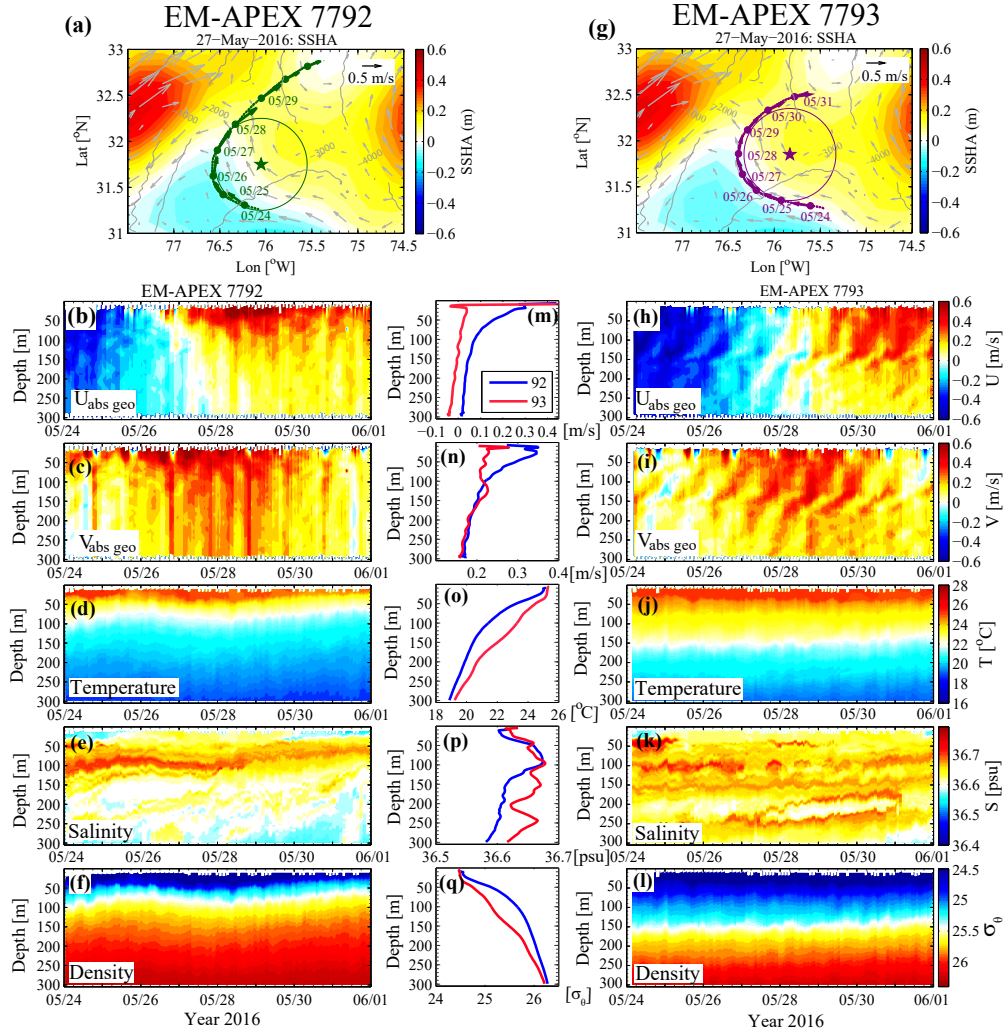
Figure 1. Observations from EM-APEX floats 7792 (a–f) and 7793 (g–l). Float trajectories are fitted to ellipses (centers shown with stars), with AVISO sea surface height and velocity. Timeseries are of zonal absolute velocity component (b, h), meridional absolute velocity component (c, i), temperature (d, j), salinity (e, k), and σ_θ (f, l). Color bars for panels (h–l) apply equally to panels (b–f). Center panels (m–q) are the time averaged profiles over the durations of the timeseries.

3. Analysis

3.1. Prominent Low-Frequency and NIW Structures

Rather than the conventional use of bandpass filtering, we use a separation of lower frequency and NIW velocity components (Figure 2) as one-half the sum and one-half the difference between velocity profiles taken 13 h, or half an intrinsic NIW period, apart; these represent the low-frequency and NIW velocity components, respectively. The times for the pairs of 13-h sum

5

and difference profiles are moved one hour and repeated for the duration of the timeseries. This method (Sanford, 1975) is a variation of a method using four profiles separated by half an inertial period. Silverthorne & Toole (2009) using four profiles in 2 inertial periods report that 98% of the NIW KE is passed by the half inertial period differences compared to a Butterworth filter with pass window ±15% of f. A prominent peak in NIW amplitude Spd_{NIW} of 0.12 m s^{-1} was observed by float 7793 at 135 m depth (Figure 2b). The phase slopes up in time (Figure 2b,e and 3a), indicating a dominantly downward propagating NIW (Leaman & Sanford, 1975).
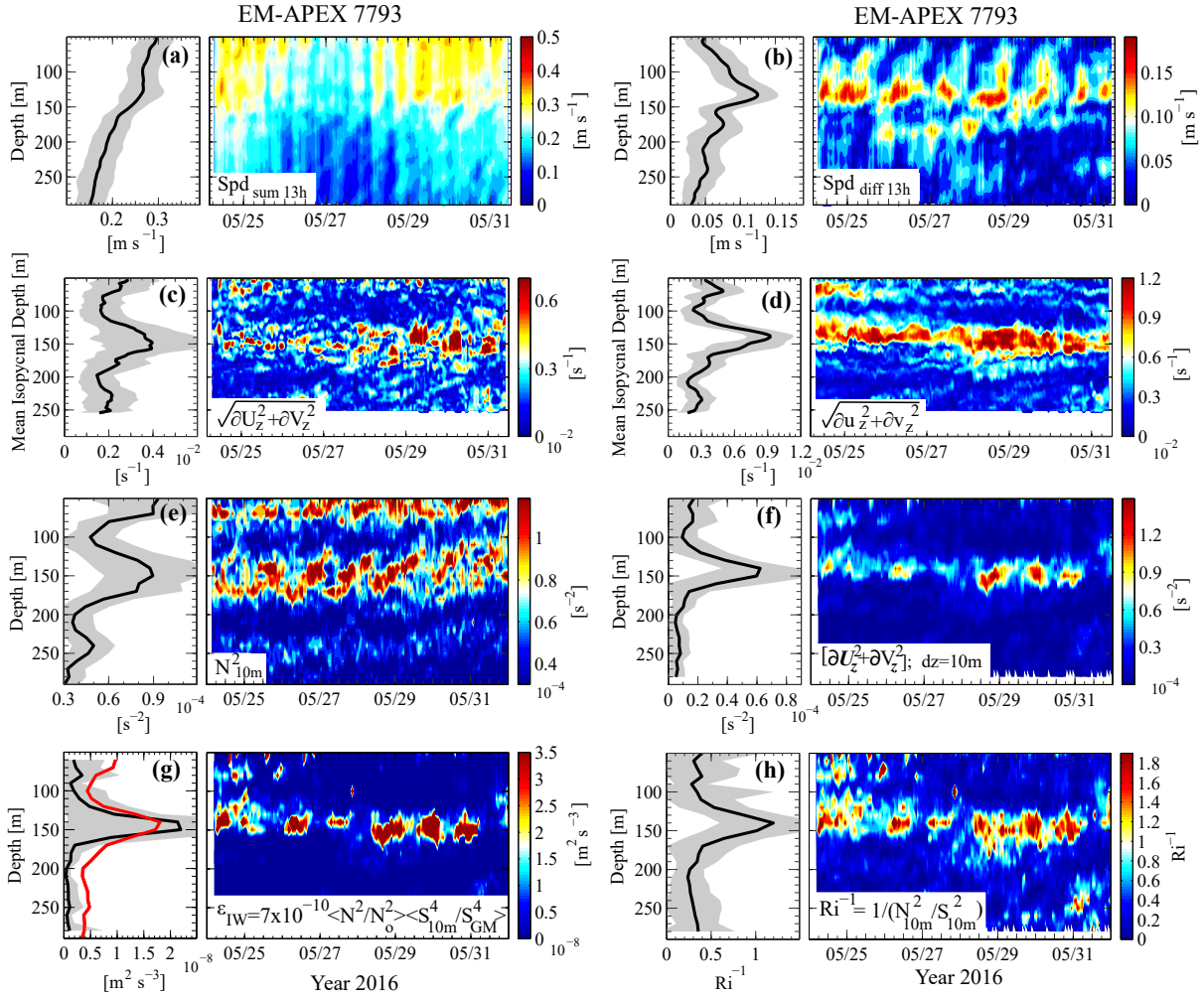

Figure 2. Float 7793 profiles displayed as averages (with std. dev.) and timeseries. The top panels (L-R) are background mean speed from the 13-h halves of the sum (a) and speed of the difference (b) profiles. The 2nd row is in semi-Lagrangian isopycnal-following coordinates of 13-h sum (c) and difference (d) shear modulus. The 3rd row is N^2 (e) and total shear squared (f; i.e., S_{10}^2). The 4th row is parameterized rate of KE dissipation ε_{IW} (g) black and 0.5 x 10^{-4} s^{-1} times TKE$_5$ in red and inverse 10-m gradient Richardson number Ri^{-1} (h). Averages of the adjacent timeseries are displayed with std. dev. levels (grey).

3.2. Shear and Kinetic Energy Dissipation Rate Profiles

The peak in 10-m shear corresponds with the peak in N^2. The upward phase modulations in N^2 (Figure 2e) are due to the NIW's vertical strain (Alford & Gregg, 2001). The inverse Richardson number Ri^{-1} over 10 m is about 1.2 (Figure 2h) and resembles the vertical structure for shear squared and rate of KE dissipation. When plotted in an isopycnal-following or "semi-Lagrangian" frame (Figure 2d; Pinkel, 1984), the shear zone is seen to descend through isopycnals. The wave's upward phase propagation and lag between its shear and strain (Winkel, 1998; Alford & Gregg, 2001; Alford et al., 2017) indicate that the NIW was propagating downward and toward the ESE.

According to Gregg (1989), KE dissipation rate (Figure 2g) is parameterized from shear and N (although based on wave-wave interactions is widely used),

$$<\varepsilon_{IW}> = 7 \text{ x } 10^{-10} <N^2/N_0^2><S^4/S_{GM}^4> \text{ W kg}^{-1}, \tag{1}$$

where N and S are buoyancy frequency and 10-m vertical shear, respectively, and ϵ_{IW} is computed for each profile for the timeseries as well as averaged (denoted by $<>$) over the duration of the timeseries. N_0 is 3 cph ($5.24 \text{ x } 10^{-3} \text{ s}^{-1}$) and S_{GM}^2 is taken to be $0.7N^2$ (Eq. 22 in Gregg, 1989). The parameterized rate of KE dissipation ε_{IW} (Figure 2g) peaks at $2.2 \text{ x } 10^{-8}$ W kg^{-1}. During the nearly LatMix field experiment, dissipation rates at 25.4 σ_θ (150 m) of $3 \text{ x } 10^{-9}$ W kg^{-1} were reported (Shcherbina et al., 2015). In the absence of energy input, a decay timescale computed from the ratio of KE to dissipation rate of KE is $5.2 \text{ x } 10^5$ s or about 6 days, comparable to past estimates by Hebert and Moum (1996) and Alford and Gregg (2001). Little change in KE was observed over our observational period, which was longer than this timescale, indicating that turbulence was possibly maintained by continued downward fluxes and/or lateral energy transfer processes.

The vertical diffusivity of density, expressed as $0.2\varepsilon_{IW}/N^2$ (Osborn, 1980), is $3.3 \text{ x } 10^{-5}$ m^2 s^{-1}. This is about one decade larger than the weak straining region observed at 25.4 σ_θ during the LatMix experiment (Shcherbina et al., 2015).

3.3. NIW Frequencies, Phase and Group Velocities, Total Energy, Vertical Energy Flux, and its Vertical Gradient

The near-inertial frequency (Figure 3c) of the 13-h velocity differences was estimated by harmonic fits to velocity component timeseries (ω_{harm}) and by the rate of NIW direction rotation vs. depth for the week-long record (ω_{rot}), a method (Fer, 2014) that provides not only mean values each 5-m but also the standard deviations. Estimation of C_{pz} as the slope of the peak values of NIW components vs. time and depth (Leaman, 1976) is subjective. Alternatively, C_{pz} is computed as ω_{rot}/m, with uncertainty based on the standard deviations of the individual components. For a single NIW, the vertical wavenumber is related to the vertical gradient of the velocity direction, i.e., $m = - d\theta_{13h}/dz$, where $\theta_{13h} = tan^{-1}(v/u)$. We interpret our

observations as a single dominant wave that undergoes vertical wavenumber changes as C_{gz} decreases (Figure 3e). The variations observed are much greater than those produced by a WKB change (Leaman & Sanford, 1975), and occur on a vertical scale comparable to that of the background changes. Hence, no WKB modification has been undertaken.

The success of determining the NIW vertical phase speed led to a direct estimate of the vertical group velocity computed as $\partial\omega_i/\partial m$ (Lighthill, 1978), which is determined as $(\partial\omega_i/\partial z)/(\partial m/\partial z)$. Demonstration of the utility of this new method, which avoids the notoriously frequency-sensitive estimation of NIW group velocity (Alford et al., 2016, 2017) is a central result of this paper. The profile of C_{gz} (Figure 3e) is downward, as expected, with a smooth trend from -4 x 10^{-4} m s^{-1} to near zero (within uncertainty) at 135 m. The NIW KE energy density (Figure 3f) is estimated as

$$E \ = \ \tfrac{1}{2}\,Spd_{13h\ diff}^2, \tag{2}$$

The energy flux (Figure 3g) and the flux divergence (h) are then simply computed from $F=C_{gz}E$.

The direct computation of vertical group velocity and, hence, its energy flux have not been reported before to our knowledge. Doing so requires some special circumstances. First, moving with the NIW pulse to observe the intrinsic frequency for a long duration with high vertical resolution is vital. Also, the frozen field hypothesis supports treating the week-long observation as a timeseries, without significant modifications along the trajectories. The direct computation of C_{gz} obviates the need to use any of the many analytic versions of a dispersion relation, which vary with the number of parameters assumed, such as $\omega, f, \zeta_0, V_0, N, k, l, m$, as required in Joyce et al. (2013) and other dispersion relations.
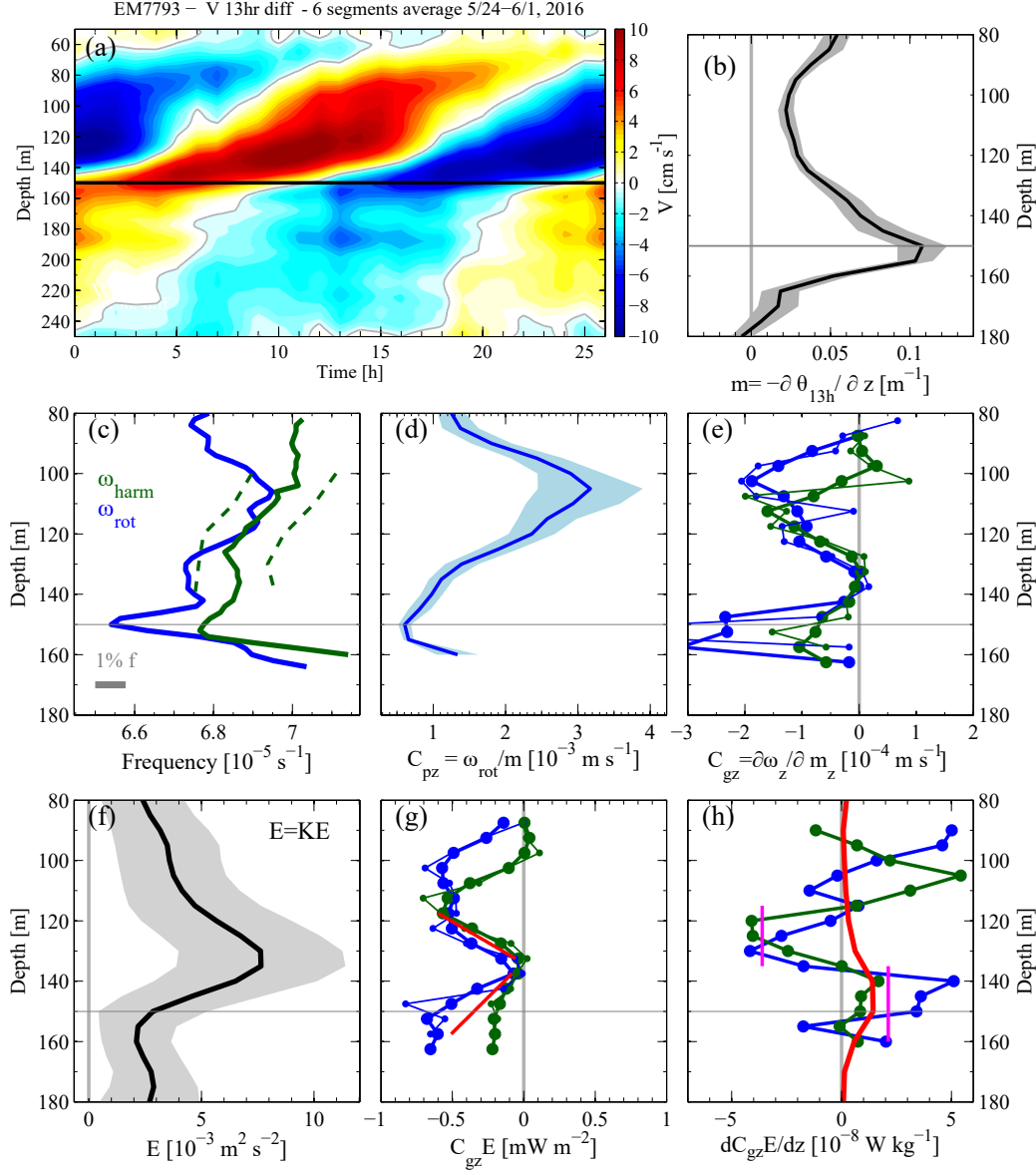
Figure 3. Analyses of float 7793 observations over about 1 week. (a) Timeseries of 13h V velocity component phase vs. depth and time vertical gradient of average of seven 25-h sections, (b) average vertical wavenumber profile m based on $-d\,\theta_{13h}(z)/dz$, (c) profiles of NIW frequency based on harmonic fit of timeseries ω_{harm} and rate of wave direction change with time ω_{rot}, (d) C_{pz} based on ω_{rot}/m, (e) C_{gz} from $\partial\omega/\partial m$ for ω_{harm} and ω_{rot}, (f) E kinetic energy, (g) $C_{gz}E$ (with a triangular filter applied – weights ¼, ½, ¼ , original data in thin lines), $C_{gz}E$, red lines are least squares fits from 110-135 m and from 135 to 160 m, (h) $dC_{gz}E/dz$ compared with rate of KE dissipation (red); magenta lines are the slopes of red lines in panel (g). Larger axes for panels e, g and h are to assist comparison with Figure 4 panels g, i, and j.

9

3.4. Observations Compared with Theory Based on Mesoscale Ocean Vertical Vorticity and Shear

Whitt and Thomas (2013) renewed consideration of mesoscale vorticity (such as in a front) and baroclinicity (i.e., flow with vertical shear). The formulation of NIW interactions with vorticity and vertical shear of a mesoscale eddy (Kunze et al., 1995) has been complemented by Joyce et al. (2013). The formulations deal with the phenomenon in slightly different ways. We chose to implement the Joyce et al. (2013) approach because it is more appropriate for profiler observations.

In the presence of sloping isotherms, the minimum NIW frequency is determined by the eddy vorticity and by the baroclinicity. The latter is denoted as Ri_g, the geostrophic Richardson number. NIWs are influenced both by the profiles of vertical vorticity ζ_0 and the azimuthal velocity V_0 at radius r_0, the difference between ζ_0 and $2V_0/r_0$ is evidence of non-solid-body rotation. Joyce et al. (2013) express their minimum frequency as:

$$\sigma_{min}^2 = \sigma_f^2 - f^2/Ri_g, \tag{3}$$

where

$$\sigma_f^2 = (f + 2V_0/r_0)(f + \zeta_0). \tag{4}$$

The vertical group velocity can be expressed in terms of vertical phase velocity via the dispersion relation for internal waves (Eqn. 49 of Whitt & Thomas, 2013):

$$C_{gz} = -C_{pz}\left(\omega^2 - \sigma_f^2 - M^2\frac{l}{m}\right)/\omega^2. \tag{5}$$

The NIW phase slope is $\frac{l}{m}$, where

$$\frac{l}{m} = -M^2/N^2 \pm \sqrt{(\omega^2 - \sigma_{min}^2)/N^2} \text{ and} \tag{6}$$

$$Ri_g = f^2N^2/M^4 \text{ with } M^2 = (f + \zeta_0)\,\partial V_0/\partial z. \tag{7}$$

The estimates of the above quantities and the resulting KE flux and its divergence are presented in Figure 4.
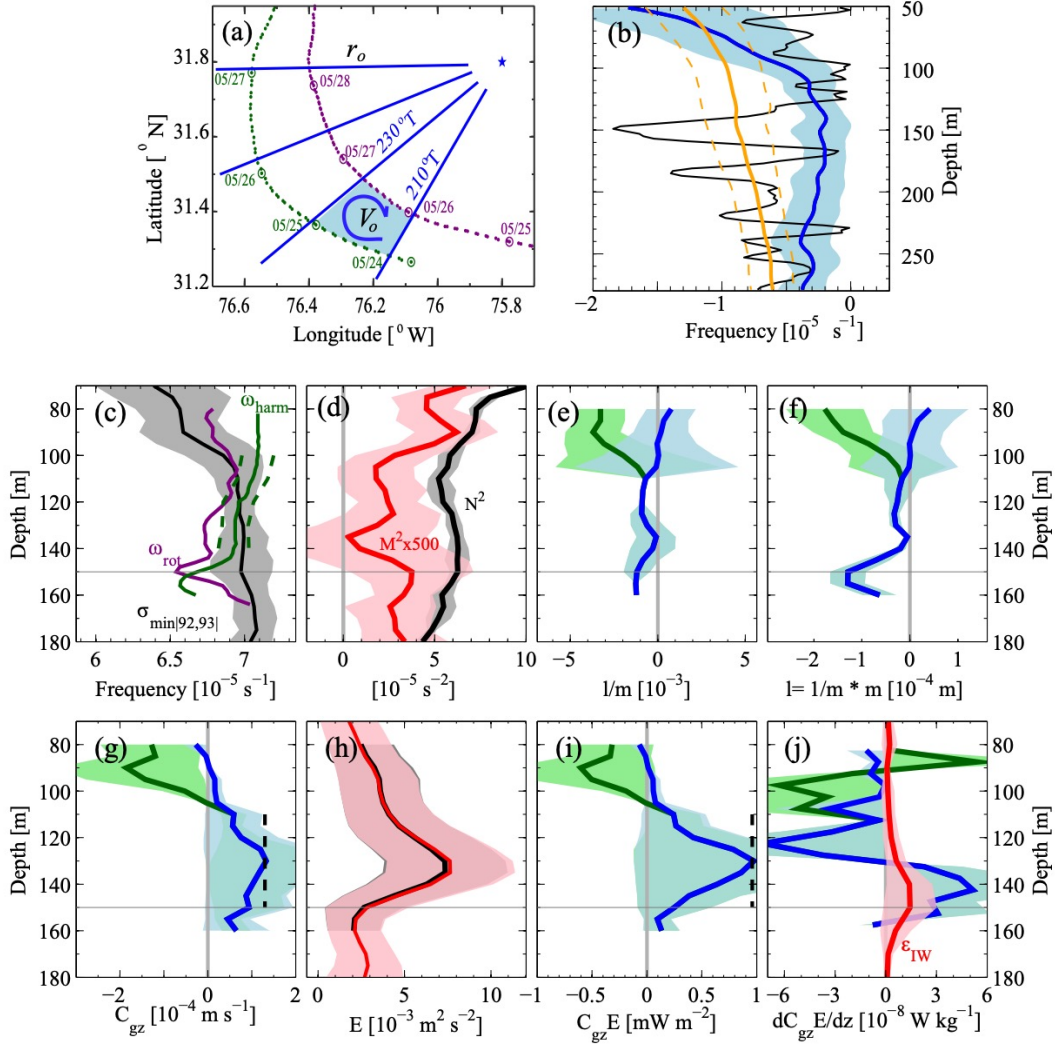
Figure 4. Evaluation of terms in the Joyce et al. (2013) formulations for a NIW in an anticyclonic mesoscale ocean eddy applied to floats 7792 (green) and 7793 (red) observations. (a) Computation of vorticity by applying the Kelvin circulation theorem in 20° boxes and areal average velocity divided by box-center r. Panel (b) displays mean and std. dev. For vertical vorticity ζ_0 (blue), vorticity profiles computed as $2V_0/r_0$ (orange), and $\sqrt{f^2/Ri_g}$ (black, plotted negative to fit on panel) with shading or dashed lines for std. dev. Panel (c) is the comparison of ω_{harm} (green), ω_{rot} (purple) and σ_{min} (black). .Panel (d) are the quantities in (7), Panel (e) is the slope of the NIW characteristics from (6), Panel f is the NIW's vertical wavenumber, Panel (g) is the wave's vertical group velocity computed from (5) (blue is for plus sign and green is minus sign of the square root term in (6)) with dashed line where zero is the observed depth of stalling. Panel (h) KE profile, Panel (i) is the vertical energy flux with dashed line as shown in panel (g). Panel (j) is the vertical convergence of the energy flux. Refer to Figure 3d for profile of vertical phase speed.

11

The vorticity profiles ζ_0 and $2V_0/r_0$ are computed in areas bounded by radials spaced 20° apart in azimuth and the radial distances between profiler tracks (Figure 4a). The 20° boxes are advanced 1° in azimuth between computations. Similarly, other large-scale representations of the region, such as M^2, N^2 and Ri_g are also averages of variables from both floats in the 20° boxes. Vorticity and f^2/Ri_g are plotted in Figure 4b, with the associated minimum frequency computed from (3) shown in Figure 4c. M^2 and N^2, wave charactistic slope l/m, m, vertical group velocity, KE density, KE vertical flux and KE vertical flux divergence are then shown in Figure 4g-j. The profiles of C_{gz} and $C_{gz}E$ (Figure 4g, i) agree well with the directly observed estimates (Figure 3f, g) in structure, showing lagged cross correlations of 0.83 and 0.85 for ω_{rot} and ω_{harm}, respectively. Modeled C_{gz} and $C_{gz}E$ exhibit offsets at the observed stalling depth by 1.3 x 10^{-4} m s^{-1} and 1 mW m^{-2} for $C_{gz}E$, and by 5 m in depth, well within the model uncertainty.

4. Discussion and Conclusions

In a novel experiment, a pair of velocity and density profiling floats in an anticyclonic ocean eddy reveal vertical and lateral water properties and kinematics that influence the propagation and stability of NIWs. Float 7793 moved nearly with a zone of turbulence, providing profiles of the intrinsic wave frequency ω and vertical wavenumber m. Float 7792, on a nearly concentric trajectory, did not observe the NIW but did contribute to the estimates of ζ_0 and V_0 in the areas between the floats. Vertical phase velocity $C_{pz} = \omega/m$ and vertical group velocity $C_{gz} = \partial\omega/\partial m$ are computed from float 7793. The strength of the direct computation of C_{pz} and C_{gz} from a single profiling float is having no reliance on numerous inferred parameters (e.g., ζ_0, V_0, N, k, l). Moreover, the observational requirements lead us to believe this analysis has not been applied to field observations before.

To the extent possible, a 1D analysis is considered. For steady NIW properties and quasi-Lagrangian measurements, the dominant terms in the vertical turbulent KE flux balance are taken to be

$$0 \cong -\partial C_{gz}E/\partial z + \mathcal{P} - \varepsilon(1 + \Gamma), \tag{8}$$

where on the RHS the terms are vertical gradient of the KE flux, turbulent shear production, and rate of KE dissipation with the addition of the mixing efficiency Γ, which is generally taken to be 0.2 (Gregg et al., 2019)

The vertical group velocity in Figure 3 is downward and decreases from -1.3 x 10^{-4} m s^{-1} (11 m d^{-1}) at 110 m to about zero by 135 m. KE increases strongly from 115 m to a peak at 135 m. The vertical energy flux is about -0.5 mW m^{-2} at 110 m and nearly -0.05 mW m^{-2} at 135 m depth. This convergent energy flux (Figure 3h, blue/green) is larger than, but of the same order of magnitude, as dissipation from 115-m depth to a maximum at 135 m (Figure 3h, red). Lateral

fluxes, as suggested by Figure 1 in Kunze et al. (1995), are likely also important. Regardless, a central finding of our work, through direct estimation of NIW group velocity, is that stalling at the base of a mesoscale feature increases the wave's KE, vertical wavenumber, shear and Ri^{-1} – which initiates and supports dissipation in the same depth range.

Below 135-m depth the vertical energy flux is divergent, but dissipation is uniform to 150 m and tapers to zero at 170 m. Caution may be needed in interpreting group velocity in a region of dissipation, as we have done (though the dissipation timescale is 6 wave periods, suggesting a minor effect on the wave's energetics). Using our method, the estimate of the vertical energy flux is -0.05 mW m^{-2} at 135 m and -0.4 mW m^{-2} below 150 m. Although of uncertain value, this divergent flux term cannot be source for dissipation, because it and ϵ are of the same sign in the turbulent KE flux balance equation (8). A prime candidate is the shear production term $\mathcal{P}$ (e.g., $-<uw><\partial U/\partial z>$). Tennekes and Lumley (1972) emphasize the importance of Reynolds stresses in the production of turbulence. The spatial correlation of TKE$_5$ and ϵ supports this interpretation. Pope (2000, Table 5.4) reports that in unstratified water,

$$-<uw> = 0.28 - 0.33 <uu>. \tag{9}$$

An estimate of Reynolds stress production based on TKE$_5$ could support the KE dissipation rate with a coefficient about a decade smaller. A smaller coefficient is expected, as w is reduced in stratified water. This hypothesized source for ϵ will be examined in the future, especially with the turbulence-measuring EM-APEX floats (Lien et al., 2016). We acknowledge that we do not know the exact interpretation of TKE$_5$, such as in terms of $<u^2 + v^2>_5$.

The Joyce et al. (2013) theory agrees well with the observations of NIW–mesoscale eddy interactions and provides an intuitive diagnosis of the interactions. The pair of floats moving with the turbulent zone on concentric trajectories provide ζ_0 and $2V_0/r_0$ and vertical shear, which are essential to a comparison with the theory of Joyce et al. (2013). The differences between ζ_0 and $2V_0/r_0$ strongly influenced the model computations. In spite of offsets between modeled and observed group velocity and energy flux profiles, the theory supports our interpretation of NIW stalling.

Initially, the goal of the study was to use observations in the Joyce et al. (2013) model to determine if it reproduced stalling at 135 m. It became clear that the observations were suitable for computations of wave properties based on first principles, without recourse to a dispersion relation. This first of its kind analysis, is a credible standard for comparison with the model. More comprehensive field studies, such as arrays of profilers, as the 20 used in Lien and Sanford (2019), should be able to observe the full 3D and temporal behavior of NIW within mesoscale eddies, which trap and dissipate NIWs globally (Whalen et al., 2018).

References

Alford, M. H. (2010). Sustained, full-water-column observations of internal waves and mixing near Mendocino Escarpment, *Journal of Physical Oceanography, 40,* 2643-2666.

Alford, M. H. & Gregg M. C. (2001). Near-inertial mixing: modulation of shear, strain and microstructure at low latitude, *Journal Geophysical Research Oceans*, *106,* 16,947-16,968.

Alford, M. H., MacKinnon, J. A., Simmons, H. L. & Nash, J. D. (2016). Near-inertial internal gravity waves in the ocean, *Annual Review of Marine Science*, *8*, 95-123.

Alford, M. H., MacKinnon, J. A., Pinkel, R & Klymak, J. M. (2017). Space-time scales of shear in the North Pacific, *Journal of Physical Oceanography, 47,* 2455- 2478.

D'Asaro, E. A., (1985). The energy flux from wind to the near-inertial motions in the surface mixed layer, *Journal of Physical Oceanography, 15*, 1043-1059.

D'Asaro, E.A. & Perkins, H. (1984). A near-inertial wave spectrum for the Sargasso Sea in late summer, *Journal of Physical Oceanography, 14*, 489-505.

Drever, R.G. and Sanford, T. B. (1970). A free-fall electromagnetic current meter - instrumentation. Conference on Electronic Engineering in Ocean Technology, University College, Swansea, 21-24 September 1970. *I.E.R.E. Conference Proceedings 19,* 353-370. Reprinted *in The Radio and Electronic Engineer 41*: 375-383.

Garrett, C. (2001). What is the ''Near-Inertial'' Band and Why Is It Different from the Rest of the Internal Wave Spectrum? *Journal of Physical Oceanography, 31*, 962-971.

Gregg, M. C. (1989). Scaling turbulent dissipation in the thermocline, *Reviews of Geophysics, 94*, 9686-9698.

Gregg, M. C., D'Asaro, E.A., Riley, J. J. & Kunze, E. (2019). Mixing efficiency in the ocean. *Annual Review of Marine Science, 10(9),* 443-473.

Hebert, D. & Moum, J. N. (1994). Decay of a near-inertial wave, *Journal of Physical Oceanography, 24*, 2334–2351.

Hsu, Je-Yuan, Lien, Ren-Chieh, D'Asaro, Eric A, & Sanford, T. B. (2018). Estimates of Surface Waves Using Subsurface EM-APEX Floats under Typhoon Fanapi 2010, *Journal of Atmospheric and Oceanic Technology*, *35*, 1053-1075

Joyce, T., Toole, J., Klein, P. & Thomas, L. (2013). A near-inertial mode observed within a Gulf Stream warm-core ring, *Journal Geophysical Research Oceans*, *118,* 1797–1806.

Kawaguchi, Y, Nishino, S., Inoue, J., Maeno, K, Takeda, H. & Oshima, K. (2016). Enhanced diapycnal mixing due to near-inertial internal waves propagating through an anticyclonic eddy in the ice-free Chukchi Platform, *Journal of Physical Oceanography, 46,* 2457-2481.

Kawaguchi, Y, Wagawa, T. & Igeta, Y. (2020). Near-inertial internal waves and multiple-inertial oscillations trapped by negative vorticity anomaly in the central Sea of Japan, *Progress in Oceanography, 181*, 202240.

Kunze, E. (1985). Near-inertial wave propagation in geostrophic shear, *Journal of Physical Oceanography, 15*, 544–565.

Kunze, E., Schmitt, E. R., & Toole, J. M. (1995). The energy balance in a warm-core ring's near-inertial critical layer, *Journal of Physical Oceanography, 25,* 942-957.

Kunze, E., & Sanford, T. B. (1984). Observations of near-inertial waves in a front, *Journal of Physical Oceanography, 14,* 566–581.

Kunze, E. & Lueck, R. (1986). Velocity profiles in a warm-core ring. *Journal of Physical Oceanography*, *16,* 991-995.

Kunze, E. & Toole, J. M. (1997) Tidally-driven vorticity, diurnal shear and turbulence atop Fieberling Seamount. *Journal of Physical Oceanography*, **27**, 2663-2693.

Leaman, K.D. (1976). Observations of vertical polarization and energy flux in near-inertial waves, *Journal of Physical Oceanography, 6, 894-908.*

Leaman, K.D. & Sanford, T. B. (1975). Vertical energy propagation of inertial waves: a vector spectral analysis of velocity profiles. *Reviews of Geophysics, 80*, 1975-1978.

Lien, R-C, Sanford, T. B. Carlson, J. A. & Dunlap, J. H. (2016). Autonomous microstructure EM-APEX. *Methods in Oceanography, 17*, 282-295.

Lien, R.-C. & Sanford, T. B. (2019). Small-scale potential vorticity in the upper ocean thermocline. *Journal of Physical Oceanography*, *49*, 1845-1872.

Lighthill, M.J. (1978). *Waves in Fluids*. Cambridge University Press, Cambridge UK. 504pp

Mooers, C. N. K. (1975). Several effects of a baroclinic current on the cross-stream propagation of inertial-internal waves, *Geophysical Fluid Dynamics*, *6*, 245–275.

Osborn, T. R. (1980). Estimates of the local rate of vertical diffusivity from dissipation measurements, *Journal of Physical Oceanography, 19*, 83-89.

Pinkel, R. (1984). Doppler observations of internal waves: the wavenumber-frequency spectrum, *Journal of Physical Oceanography, 24*, 1249-1270.

Pinkel, R., Goldin, M. A., Smith, J. A., Sun, O. M., Aja, A. A., Bui, M. N. & Hughen, T. (2011). The wirewalker: A vertically profiling instrument carrier powered by ocean waves, *Journal of Atmospheric and Oceanic Technology*, *28*, 426–435.

Pope, Stephen B. (2000) Turbulent Flows, Cambridge University Press.

Rossby, H. T. (1969). A profile of current near Plantagenet Bank. *Deep-Sea Research, 16*, 766,774.

Rossby, H. T. & Sanford, T. B. (1976), A study of velocity profiles through the main thermocline. *Journal of Physical Oceanography, 6***,** 776-778.

Sanford, T. B. (1971). Motionally induced electric and magnetic fields in the sea, *Reviews of Geophysics, 76*, 3476-349.

Sanford, T. B., (1975). Observations of the vertical structure of internal waves, *Reviews of Geophysics, 80*, 3861-3871.

Sanford, T. B., (2013). Spatial structure of thermocline and abyssal internal waves, *Deep-Sea Research Part II*, *85*, 195-209.

Sanford, T. B., Drever, R. G. & Dunlap, J. H. (1978). A velocity profiler based on the principles of geomagnetic induction, *Deep-Sea Research, 25*, 183-210.

Sanford, T. B., Dunlap, J. H., Carlson J. A. & Girton, J. B. (2005). Autonomous velocity and density profiler: EM-APEX, *Proc. Eighth Working Conference on Current Measurement Technology*, 152-156. **DOI:** 10.1109/CCM.2005.1506361

Sanford, T.B, Price, J. F., Girton, J. B. & Webb, D. C. (2007). Highly resolved observations and simulations of the ocean response to a hurricane. *Geophysical Research Letters,* **34***,* L13604, doi:10.1029/2007GL029679.

Shcherbina, A. Y., Sundermeyer, M. A., Kunze, E., , D'Asaro, E., Badin, G., Birch, D., Brunner-Suzuki, A.-M. E. G. et al. (2015). The LatMix summer campaign: Submesoscale stirring in the upper ocean, *Bulletin American Meteorology Society, 96*, 1257–1279.

Silverthorne, K.E. & Toole, J. M. (2009). Seasonal kinetic energy variability of near-inertial motions, *Journal of Physical Oceanography, 39*, 1035-1049.

Spain, P. F., Dorson, D. L. & Rossby, H. T. (1981). PEGAGUS: A simple, acoustically tracked, velocity profiler. *Deep-Sea Research, 28*,1553-1367.s

Tennekes, H. & Lumley, J.L. (1972). A First Course in Turbulence, The MIT Press, Cambridge, MA.

Visbeck, Martin. (2002). Deep Velocity Profiling Using Lowered Acoustic Doppler Current Profilers: Bottom Track and Inverse Solutions*****, *Journal of Atmospheric and Oceanic Technology, 19,* 794-807.

Weller, R. A. (1982). The relation of near-inertial motions observed in the mixed layer during the JASIN (1978) experiment to the local wind stress and to quasi-geostrophic flow field, *Journal of Physical Oceanography, 12*, 1122–1136.

Whalen, C. B., MacKinnon, J. A. & Talley, L. D. (2018). Large-scale impacts of the mesoscale environment on mixing from wind-driven waves, *Nature Geosciences, doi.org/10.1038/s41561-018-0213-6*.

Whitt, D. B. & Thomas, L. N. (2013). Near-inertial waves in strongly baroclinic currents, *Journal of Physical Oceanography, 43*, 706–725.

Winkel, D. (1998). Influences of mean shear in the Florida Current on turbulent production by internal waves. PhD thesis, University of Washington, Seattle.